https://doi.org/10.15407/ufm.25.03.545

S.O. FIRSTOV* and T.G. ROGUL**

I.M. Frantsevich Institute for Problems in Materials Science
of the N.A.S. of Ukraine,
3 Omeljan Pritsak Str., UA-03142 Kyiv, Ukraine

* sfirstov@ukr.net, s.firstov@ipms.kyiv.ua; ** rogul.tamara@gmail.com

FEATURES OF SOLID-SOLUTION HARDENING AND TEMPERATURE DEPENDENCE OF THE CRITICAL SHEAR STRESS IN BINARY AND MULTICOMPONENT ALLOYS

The paper analyses the hardening of binary and multicomponent solid solutions (including high-entropy alloys (HEAs)); addresses the notion of a compositional–cluster structure of binary solid solutions with unlimited solubility to propose an equation describing the concentration dependence of the critical shear stress; presents findings from a comparative analysis of the temperature dependences for critical shear stress (yield stress) for a series of binary and multicomponent solid solutions and pure metals with b.c.c. and f.c.c. lattices; considers potential mechanisms, which lead to a 'plateau' on the temperature dependence of critical shear stress for binary and multicomponent solid solutions and for pure metals; discusses the specifics of athermal hardening of HEAs and proposes a relatively simple equation for assessing their athermal hardening; and addresses the capabilities of using the x-ray diffraction to determine the root-mean-square displacements of atoms from ideal positions at crystal-lattice sites, $\sqrt{U^2}$, and crystal-lattice microdistortions, ε, in multicomponent solid solutions.

Keywords: binary and multicomponent alloys, solid-solution hardening, yield stress, critical shear stress.

Citation: S.O. Firstov and T.G. Rogul, Features of Solid-Solution Hardening and Temperature Dependence of the Critical Shear Stress in Binary and Multicomponent Alloys, *Progress in Physics of Metals*, **25**, No. 3: 545–569 (2024)

1. Introduction

The development of models describing solid-solution hardening of binary solid solutions is addressed in numerous papers. These papers have been analysed and summarised in sufficient detail in various monographs and overviews (*e.g.*, [1–6]). Nevertheless, recent years have seen a growing interest in exploring the mechanisms of solid-solution hardening in multicomponent solid solutions. This surge in interest is attributed to the intensive research into a new class of materials, namely high-entropy alloys (HEAs), whose creation was advanced by J.W. Yeh in 2004 [7].

The development of HEAs relies on a fundamentally new scientific approach that emphasizes the predominant role of mixing entropy in forming a solid solution in multicomponent alloys. HEAs contain at least five key elements, each having an atomic concentration ranging from 5 to 35% and possessing high mixing entropy. The minimization of the Gibbs free energy $G = H - TS$, where H is the enthalpy, S is the entropy, and T is the absolute temperature, promotes the formation of single-phase multielement substitutional solid solutions with simple lattices (b.c.c., h.c.p., and f.c.c. ones). The HEA crystal lattice, constituted by atoms varying in size and electronic structure, is significantly distorted, giving rise to a spectrum of unique properties.

Principles for selecting the elemental composition of HEAs with the desired type of crystal lattice have been established, and studies are ongoing to ascertain the influence of their elemental composition on the structure and mechanical properties (see, *e.g.*, [8–20]). It is shown (*e.g.*, [8–14])) that HEAs are distinguished by enhanced thermal stability, slow diffusion kinetics, and high wear and corrosion resistance. Consequently, they are expected to be successfully used as structural materials in current and future industrial applications.

Specifically, a series of studies highlighted the potential of developing HEAs that could compete with today's leading high-temperature creep-resistant polycrystalline alloys (such as Inconel 718 and Haynes 230) [19, 20, 21]. For example, Yeh [20] examined a series of HEAs in the Al–Co–Cr–Fe–Ni–Ti system that possesses high creep resistance, good oxidation resistance, and low specific weight (below 8 g/cm^3). It is also important that costs for raw materials for such systems are approximately 20% lower than for conventional nickel-based superalloys. The paper [21] presents the promising Al10Co25Cr8Fe15Ni36Ti6 alloy, showing a strength limit of 650 MPa at 800 °C, which is higher than that of Inconel 617 (strength limit lower than 500 MPa).

However, there are several issues to be solved in terms of developing novel multicomponent high-entropy structural and functional materials. Primarily, mechanisms of abnormally high solid-solution hardening pertinent to HEAs are to be ascertained [16, 18]. Thus, it is noted [16] that the

high hardness (5.25 GPa) of the single-phase WNbMoTaV alloy with a b.c.c. lattice can be due to the activation of an 'unobvious strengthening mechanism'. Despite a fairly large number of studies focusing on the features peculiar to solid-solution hardening and its estimation for HEAs [22–28], the mechanism of such hardening remains to be fully determined. Systematic analysis of the temperature dependence of critical shear stress τ_{cr} in solid solutions is also of special interest: in particular, long-term athermal hardening, leading to a characteristic 'plateau' on the $\tau_{cr}(T)$ dependence at temperatures above $(0.2–0.35)T_{melt}$. The findings of this analysis are noteworthy not only for their scientific value but also important for the design of creep-resistant HEAs.

To systematize the literature results and our research findings, this paper consistently addresses the mechanisms of solid-solution hardening in binary and multicomponent solid solutions (HEAs) and presents a comparative analysis between the temperature dependences of critical shear stress for binary and multicomponent solid solutions and 'pure metals'.

2. Concentration Dependence of Solid-Solution Hardening in Binary Solid Solutions

Solid-solution hardening (SSH) is known to result from the resistance to the movement of dislocations by atoms of doping elements present in the matrix lattice [1–3].

The models of Mott and Nabarro [1], Friedel [2], Fleischer [5, 29], Labusch [30], and Suzuki [31] are discussed most comprehensively in the literature to describe the solid-solution hardening in binary solid solutions. Quite a detailed analysis of the theories and models is presented, *e.g.*, in Refs. [2, 3, 6].

In essence, the proposed solid-solution hardening models are similar: they actually focus on athermal (temperature-independent) hardening, assuming that dislocations behave as elastic lines and the solid-solution hardening is primarily due to the size mismatch between the atoms of the doping element and the matrix and the difference in their elastic moduli.

In terms of the interaction between dislocations and dissolved atoms, the models presented in the literature can be conditionally divided into two categories: (i) interaction at low concentrations of dissolved atoms, when the dissolved atoms are regarded as individual point obstacles to the movement of dislocations and the moving dislocations bend in the regions between them and break away under the influence of additional stresses (Fleischer and Friedel) (Fig. 1, *a*), and (ii) interaction at high concentrations of impurity atoms, when their strain fields overlap and the dislocations interact with these fields but not with isolated atoms (Mott–Nabarro) (Fig. 1, *b*). An intermediate range of impurity-atoms' concentrations includes Labusch's model describing the interaction of a dislocation with a

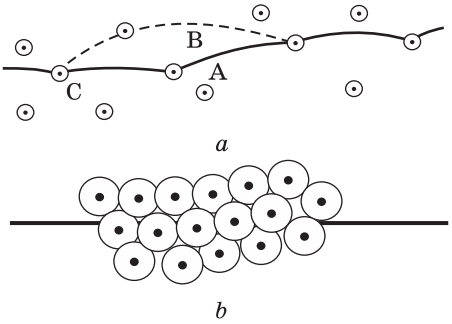

Fig. 1. Interaction of dislocations with dissolved atoms according to the Mott–Nabarro theory (atoms are shown with dots and their stress fields are shown with circles): (*a*) diluted solution under the action of additional stresses (dislocation separation from *A* atoms to *B* atoms); (*b*) concentrated solution [4]

group of closely spaced atoms (cluster) and its subsequent bending in the region between this group.

According to Mott and Nabarro [1], the movement of dislocations is hindered by internal lattice distortions induced by atoms of the dissolved element, whose sizes depend on the difference in the atomic sizes of the solvent and the dissolved element, which is the size mismatch parameter δ_a defined as the change in the lattice constant with the concentration of the dissolved doping elements c ($\delta_a = a^{-1}da/dc$). As the concentration of impurities increases, the distance between the dislocation anchor points, being inversely proportional to the atomic concentration c of the doping element, decreases, while the critical stress of dislocation separation τ increases. At high concentrations of impurity atoms, the strain fields overlap (Fig. 1, *b*) and the long-range stress fields interacting with the dislocation are the algebraic mean of the stress fields of the impurity atoms and are equal to zero. This makes the dislocations located in clusters of impurity atoms rectilinear, and their interaction with impurity atoms is primarily limited to the nuclei [4]. Based on several assumptions, Mott and Nabarro derived an equation for calculating the solid-solution hardening, $\Delta\tau$, for concentrated binary solid solutions ($c > 0.1$ at.% according to [32]):

$$\Delta\tau = 2.5G\delta_{\alpha}^{1/4}c, \qquad (1)$$

where G is the shear modulus, δ_a is the atomic mismatch parameter, and c is the concentration of the doping element.

Fleischer's model [5, 29] focuses on the interaction of dislocations with individual dissolved atoms in the slip plane and addresses, unlike Mott–Nabarro model, not only the atomic size mismatch between the solvent and impurity but also the mismatch in their elastic moduli. Fleischer concluded that the mismatch in elastic moduli δ_G ($\delta_G = G^{-1}dG/dc$) promoted greater hardening than the atomic size mismatch δ_a. According to Fleischer's model, solid-solution hardening $\Delta\tau$ for low-concentration solid solutions can be calculated using the following equation:

$$\Delta\tau = \frac{G\delta^{3/2}c^{1/2}}{760}, \qquad (2)$$

where $\delta = |\delta_G| + \alpha|\delta_a|$ with δ_G and δ_a being the elastic modulus mismatch and atomic size mismatch parameters, $\alpha = 3$ for screw dislocations and $\alpha = 16$ for edge dislocations.

However, the paper [33] indicates that the influence of the elastic modulus mismatch on hardening in Fleischer's theory is overestimated since the moduli for metals commonly change when dissolved atoms are added. The paper determined a correction to the calculation of the modulus mismatch between the dissolved atoms and matrix atoms. In the case of copper alloys, this correction leads to a 30% reduction in the modulus mismatch in Fleischer's model.

Labusch [30] revised the alloy-hardening theory by Mott and Nabarro [1] and pointed out that a uniform distribution of doping atoms could not be found in solid solutions and that there were groups (clusters) of closely spaced atoms. These groups serve as 'effective' obstacles to the movement of dislocations, exceeding the action of individual atoms in a cluster but being weaker than the sum of their individual forces. According to Labusch's model, the level of solid-solution hardening is proportional to the concentration of the dissolved substance as $c^{2/3}$:

$$\Delta\tau = \frac{G\delta^{4/3}c^{2/3}}{550}, \tag{3}$$

where $\delta = (\delta_G^2 + \alpha^2\delta_a^2)^{1/2}$ ($3 < \alpha < 16$ for screw dislocations and $\alpha > 16$ for edge dislocations).

Hence, in a general form, the concentration dependence of solid-solution hardening $\Delta\tau$ for binary solid solutions can be represented as

$$\Delta\tau(c) = BGc^n, \tag{4}$$

where τ is the critical shear resistance, B is a constant that depends on the modulus and size mismatch parameters between the atoms that form the solid solution, and c is the concentration of the doping element.

At the same time, models with $n = 1/2$ (Fleischer) perform better in the region of low concentrations of solute atoms, $n = 2/3$ (Labusch) when a dislocation interacts with a group of closely spaced solute atoms (clusters), and $n = 1$ (Mott) in transition to higher concentrations. Note that in Suzuki's approach to assessing solid-solution hardening in concentrated solid solutions with the temperature dependence of the shear modulus, $G(T)$, is taken into account that $n = 1$ [31, 34].

Therefore, with a higher content of the doping element, the concentration dependence of solid-solution hardening transfers from parabolic to linear. This transition is schematically shown in Fig. 2 [35]. The bend is clearly visible experimentally, for example, on the concentration dependence of hardness for the Mo–W alloy at 4 at.% W [32]. The models leading to parabolic and straight-line dependences are compared in [36].

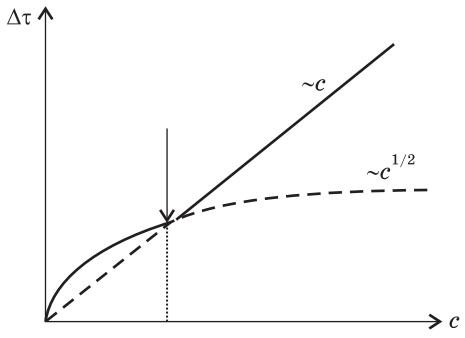

Fig. 2. Schematic dependence of solid-solution hardening $\Delta\tau$ on the concentration c of the doping element with the transition from parabolic to linear shape [35]

The concentration dependence of solid-solution hardening $\Delta\tau(c)$ in binary solid solutions with unlimited solubility of the components, which have the same lattice type and slightly differing atomic sizes and whose hardening reaches a maximum at 50% doping element (Fig. 3) Seeger [37] described as

$$\Delta\tau(c) = Ac(1 - c), \tag{5}$$

where A = const.

G. Sachs and J. Weerts [38] described the complete expression $\tau(c)$ of the Au–Ag solid solution as

$$\tau(c) = c\tau_{Ag} + (1 - c)\tau_{Au} + c(1 - c)4\tau_0, \tag{6}$$

where τ_{Ag} and τ_{Au} are the critical shear stresses for pure Ag and Au; τ_0 is the deviation from the values of the critical shear stress calculated according to the mixture rule for 50 at.% of Ag and 50 at.% of Au.

The paper [39] notes that Eqs. (5) and (6) were derived for ideal (homogeneous) binary solid solutions with unlimited solubility, while actual solid solutions might be characterized by some concentration heterogeneity. It is assumed that a binary solid solution with unlimited solubility of components can be represented as a mixture of areas (clusters) enriched in component A and enriched in component B since atoms of the doping element are unevenly distributed in the alloy. This 'composite' is peculiar in that there is no physically clear boundary that separates these areas (Fig. 4).

Assuming that the solid solution has a compositional cluster structure, the paper [39] proposed the following equation to describe the concentration dependence of critical shear stress $\tau(c)$ in binary solid solutions with unlimited solubility:

$$\tau(c) = [(\tau_A + \alpha_1 c(1 - c)](1 - c) + [\tau_B + \alpha_2(1 - c)c]c, \tag{7}$$

where τ_A and τ_B are the critical shear stresses of pure components A and B, α_1 and α_2 are hardening coefficients for the formation of solid solutions based on components A and B.

As obvious, the critical shear stress $\tau(0) = \tau_A$ at $c = 0$, $\tau(1) = \tau_B$ at $c = 1$, and $\tau(0.5) = 0.5(\tau_A + \tau_B) + 0.125(\alpha_1 + \alpha_2)$ at $c = 0.5$.

Proposed Eq. (7) is a third-order polynomial from the concentration c of component B. To find coefficients α_1 and α_2, it will suffice to take the first derivatives from the experimental dependence of critical shear stress on concentration at the initial and final points of the concentration

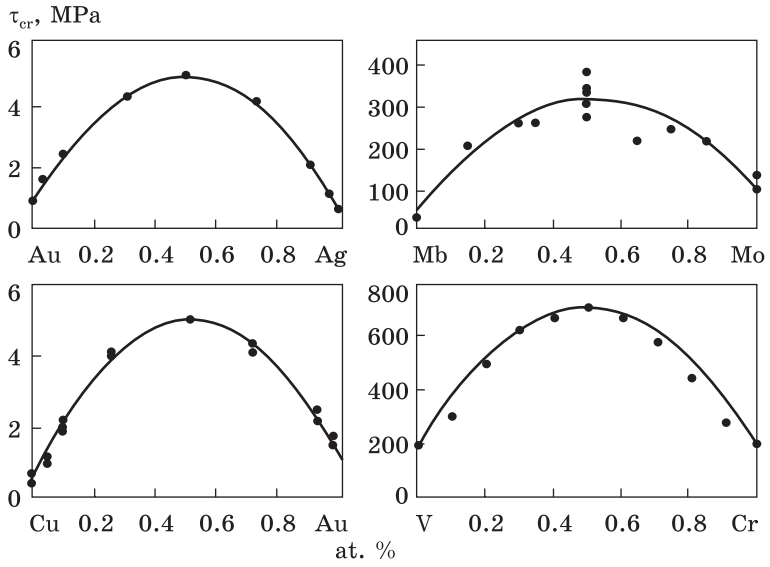

Fig. 3. Experimental data on the concentration dependences of critical shear stress $\tau_{cr}(c)$ in unlimited solid solutions of the Au–Ag [38], Cu–Au [40], Nb–Mo [41], and V–Cr [42] systems (points on the curve) and the same dependences for these systems calculated following Eq. (6) [39] (solid line)

dependences and then refine them to obtain the best match through analysis of root-mean-square deviations of the experimental data from the calculations.

To compare the dependences calculated following Eq. (7) and experimental dependences of critical shear stress on concentration, the paper [39] analysed binary solid solutions with a b.c.c. structure, Nb–Mo and V–Cr, and with an f.c.c. structure, Au–Ag and Cu–Au [38, 40–42] (Fig. 3). As shown, the calculated curves describe the experimental data well.

Summarizing the above, we should note that different explanations for the solid-solution hardening mechanisms depending on the concentration of the dissolved element are proposed within the described approaches for assessing solid-solution hardening in binary solid solutions. Nevertheless, each proposed model has its assumptions and limitations. The situation is more complicated for the hardening of multicomponent solid solutions, since the presence of a greater number

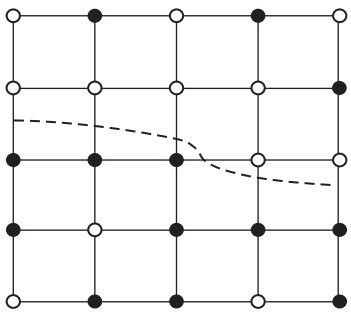

Fig. 4. Schematic compositional cluster structure of a binary solid solution: ○ (open circle) — atoms of element *A*, and ● (solid circle) — atoms of element *B* [39]

of elements leads to more complex interactions between them. Some approaches to assessing the solid-solution hardening in multicomponent solid solutions are described below.

3. Features Peculiar to Athermal Hardening of Multicomponent Solid Solutions

As noted above, differences in the atomic sizes and elastic moduli of elements in the multicomponent solid solution can lead to significant lattice distortions, significantly complicating the movement of dislocations and, accordingly, giving rise to high levels of solid-solution hardening. For this reason, the choice of both the model and the method for determining the size and elastic mismatch between the atoms of elements contained in such solutions are important in the development of approaches to calculating their hardening, since the interaction between atoms of different elements can significantly change their parameters.

A model for calculating solid-solution hardening in multicomponent alloys was first proposed by Gypen and Deruyttere far back in 1977 [43, 44]. The model uses Labusch's approach for binary solid solutions: $\Delta\tau(c) \propto c^{2/3}$. The effect of solid-solution hardening is accordingly expressed by the following equation:

$$\Delta\tau = \left[\sum_i^n B_i^{3/2} c_i\right]^{2/3}. \qquad (8)$$

Here, c_i is the concentration of an element in the alloy; $B_i = 3EZ$, where E is Young's modulus and Z depends on size mismatch δ_a and elastic mismatch δ_E between atoms of elements in the alloy. Parameter B_i in (8) is calculated for a binary solution.

To calculate solid-solution hardening of HEAs, most papers suggest approaches that also rely on the use of Labusch's model for binary solid solutions, but with different options for determining the size and elastic mismatch of atoms, *e.g.*, [22–24, 45–48].

However, the application of approaches relying on Labusch's model to calculate solid-solution hardening of HEAs does not seem to be entirely justified in our opinion. As HEAs, by definition, do not contain elements, whose concentration is lower than 5%; the solid-solution hardening of HEAs rather resembles the behaviour in concentrated solid solutions and $\Delta\tau(c) \propto c$. This is confirmed, for instance, in Refs. [49, 50]. Thus, as Ref. [49] shows, the microhardness of $(TiZrNbTa)_{100-x}Mo_x$ ($0 \le x \le 20$) HEAs produced by arc melting increases linearly with molybdenum concentration that is similar to the case of a concentrated binary solid solution. The paper [50] established that the yield stress σ of the $Al_xHfNbTaTiZr$ alloy also increases linearly with the aluminium concentration and can be described as $\sigma = 1031 + 26.1c$.

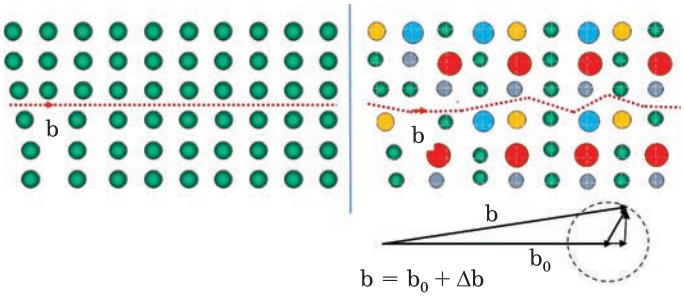

Fig. 5. Schematic movement of dislocations in a single-component crystal and in a high-entropy alloy

Using single-phase AlTiVCrNbMo and Cr MnCoFeNi alloys as an example, it is shown in Refs. [51, 52] that their abnormally high athermal solid-solution hardening is associated with a change in the Burgers vector **b** along the dislocation line (both in length and in direction). This leads to the appearance of component $\Delta\mathbf{b}$, which is perpendicular to the slip plane (Fig. 5). In this case, the full Burgers vector is equal to

$$\mathbf{b} = \mathbf{b}_0 + \Delta\mathbf{b}. \tag{9}$$

These alloys are single-phase substitutional solutions. The b.c.c.-lattice parameter of the AlTiVCrNbMo alloy is a = 3.128 Å, and the f.c.c.-lattice parameter of the CrMnCoFeNi alloy is a = 3.603 Å. The alloys have a polyhedral structure with grain sizes of 200–700 μm, the grains are quite evenly distributed by orientation, and internal stresses are virtually zero. In the early deformation stages, the sublattice of the f.c.c. CrMnCoFeNi alloy is characterized by stacking faults and twins, being indicative of low energy of stacking faults in the alloy.

As shown in Refs. [51, 52], the hardness of the AlTiVCrNbMo and CrMnFeCoNi alloys, H_{exp}, significantly exceeds (by ΔH) the hardness calculated according to the rule of mixture, H_{mix}. According to Ref. [53], $H_{\text{mix}} = \sum_i^n c_i H_i$, where c_i and H_i are the concentration and hardness of an element in the alloy. For the AlTiVCrNbMo alloy, H_{exp} = 5.1 GPa and H_{mix} = = 0.95 GPa. For the CrMnFeCoNi alloy, H_{exp} = 1.66 GPa and H_{mix} = 0.72 GPa.

To assess solid-solution hardening $\Delta\tau$ (or ΔH), a relatively simple equation is proposed, which accounts for the 'average' shear modulus $G_{\text{mix}} = \sum_i^n c_i G_i$ and the 'average' size mismatch parameter $\Delta a/a = \sum_i^n c_i (a_i - a_{\text{mix}})/a_{\text{mix}}$ with $a_{\text{mix}} = \sum_i^n c_i a_i$,

$$\Delta\tau = k\frac{\Delta}{a}G_{\text{mix}} \tag{10}$$

or

$$\Delta H = k_H \frac{\Delta a}{a} G_{\text{mix}}. \tag{11}$$

It should be noted that the size mismatch parameter $\Delta a/a$ is actually equivalent to the $\Delta\mathbf{b}/\mathbf{b}$ ratio (Fig. 5).

The hardness of the alloy is then equal to

$$H = H_{\text{mix}} + \Delta H = H_{\text{mix}} + k_H \frac{\Delta a}{a} G_{\text{mix}} . \quad (12)$$

The proportionality coefficients in Eqs. (10) and (11) are related by the expression $k_H \approx 3k$, which corresponds to Tabor's equation [54] for hardness and yield stress ($\sigma_{0.2} = H/3$). Equation (12) is obeyed for several alloys at k_H values approximately equal to 1.4–1.7.

Equations (10)–(12) include the average size mismatch, $\Delta a/a = \sum_i^n c_i (a_i - a_{\text{mix}})/a_{\text{mix}}$. At the same time, several papers use, as a measure of the size mismatch, root-mean-square discrepancy of atomic sizes, $\delta = \sqrt{\sum_i^n c_i \left[(r_{\text{av}} - r_i)/r_{\text{av}}\right]^2}$, where r_i is the atomic radius of c_i i-th element in the alloy; $r_{\text{av}} = \sum_i^n c_i r_i$. It should be noted that the root-mean-square deviations are higher than the average deviation by $\approx 1.25\pi^2/2$ according to equations in Ref. [55]. Hence, this factor allows an easy transition from the average deviation to the root-mean-square one.

4. Experimental Determination of Root-Mean-Square Displacements of Atoms in Multicomponent Solid Solutions

Differences in atomic sizes and elastic moduli between the elements in a multicomponent solid solution can lead to significant shifts of atoms from their ideal lattice positions. An attempt was made in [56] to calculate the displacement of specific atoms from ideal lattice sites in multicomponent f.c.c. stainless steels to evaluate their solid-solution hardening. Computer simulation methods (in particular, molecular dynamics methods) are currently employed to predict the displacement of atoms from ideal lattice positions. However, the actual root-mean-square displacements of atoms from their ideal lattice positions, $\sqrt{U^2}$, resulting from self-organization processes, can be experimentally determined from x-ray diffraction patterns by changes in the intensity of reflections of various orders. Respective methodologies are described in Refs. [57, 58].

The experimental values of U^2 are the sum of squared static U_{s} and dynamic U_{d} displacements of atoms from ideal-lattice sites:

$$U^2 = U_{\text{s}}^2 + U_{\text{d}}^2 . \quad (13)$$

Static distortions U_{s} are due to the difference in sizes of atoms, while dynamic distortions U_{d} are due to thermal vibration of atoms. Dynamic distortions are known to grow with temperature and should increase the resistance to the movement of dislocations in almost the same way as static distortions. In this regard, the root-mean-square displacement $\sqrt{U^2}$ of atoms, including both static and dynamic components, characterizes the actual displacements of atoms in multicomponent solid solutions and can

be used to calculate the hardening of such solutions. Thus, the paper [59] indicates that the addition of elements in the Cu–Ni–Al–Co–Cr–Fe–Si system decreases the intensity of x-ray lines that is associated with the lattice distortion.

The paper [25], using the f.c.c. CrMnFeCoNi HEA as an example, shows that root-mean-square displacements $\sqrt{U^2}$ determined by x-ray diffraction and the displacement of atoms from the ideal lattice positions calculated from first principles and averaged over five elements are in good agreement (23.5 pm^2 and 25.2 pm^2, respectively). To determine the yield stress $\sigma_{0.2}$ normalized to the shear modulus G at 0 K, the following empirical equation is used in Ref. [25]:

$$\frac{\sigma_{0.2}}{G} = k^* \sqrt{U^2}\,, \tag{14}$$

where k^* is a constant.

It is shown [25] that the above approach to calculating the solid-solution hardening effect can be successfully applied to the FeCoNi, MnFeCoNi, MnCoNi, MnFeNi, CrCoNi, CrFeCoNi, and CrMnCoNi medium-entropy alloys, being a subset of the CrMnFeCoNi alloy.

It is convenient to determine U^2 from the intensities of lines (111) and (222) for f.c.c. alloys and from the intensities of lines (110) and (220) for b.c.c. alloys, allowing the effect of texture to be excluded. In this instance, the root-mean-square shifts are apparently determined in the direction perpendicular to these planes, which is consistent with the ideas set forth in Refs. [51, 52] regarding the Burgers vector component $\Delta\mathbf{b}$ that is induced by severe lattice distortions and is normal to the slip plane, and actually define the value of this component. Accordingly, instead of expression $\Delta a/a$, being present in Eq. (10) and characterizing only the 'average' size mismatch of atoms in the crystal lattice, we propose to use $\sqrt{U^2}$ normalized by d_{hkl}, where d_{hkl} is the interplanar distance. Then Eq. (10) reads as

$$\Delta\tau = k_1 G \frac{\sqrt{U^2}}{d_{hkl}}, \tag{15}$$

where k_1 is a constant, which also accounts for the factor for conversion from the average displacement of atoms in the crystal lattice to the root-mean-square shift (≈1.25 [55]).

At the same time, it is shown [60] that there is a linear relationship between the root-mean-square displacements of atoms $\sqrt{U^2}$ and lattice microdistortions ε for solid solutions. Lattice microdistortions ε are balanced within individual crystallites or their parts (mosaic blocks) and, along with the sizes of coherent scattering domains (CSDs), lead to the broadening of x-ray lines in comparison with the reference sample lines: $\varepsilon = \Delta d/d$, where Δd is the maximum deviation of the interplanar spacing for a given interference line from its average value d.

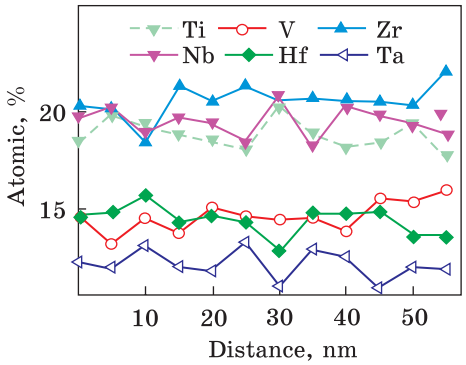

Fig. 6. Chemical inhomogeneity of the cast TiVZrNbHfTa alloy [62]

Our paper [61] established a relationship between the level of solid-solution hardening ΔH, the amount of lattice microdistortions ε, and the elastic modulus E:

$$\Delta H = \alpha \varepsilon E , \qquad (16)$$

or, according to [53],

$$\Delta\tau = \frac{\alpha}{3}\varepsilon E , \qquad (17)$$

where $\alpha \approx 22$.

The data obtained in [61] support the fact that, under precise determination of microdistortions ε, this value can be regarded as a measure of solid-solution lattice distortion and can be used to assess the level of solid-solution hardening.

It should be noted that not only high-entropy and medium-entropy alloys, but also binary solid solutions are characterized by a situation, where, to one degree or another, not a single atom is located exactly in a node of the crystal lattice. Therefore, normalized to the interplanar distance, empirically determined mean square displacements of atoms from ideal positions are $\sqrt{U^2}/d_{hkl}$ is the most correct measure of crystal lattice distortions. Another acceptable measure of such distortions can be the microdistortion values of the crystal lattice ε.

The cluster structure characteristic of binary solid solutions is even more characteristic of multicomponent solid solutions. For example, the microinhomogeneity of the distribution of the elements of the high-entropy TiVZrNbHfTa coating was clearly observed in Ref. [62]. In this case, the size of the clusters is of 15–20 nm (Fig. 6). However, if it was possible to propose a compositional–cluster model (reviewed above, [39]) for binary solid solutions for the evaluation of solid-solution strengthening, such a model has not yet been developed for multicomponent solutions.

The maximum lattice distortions may occur not only in the HEAs, but also in properly chosen medium-entropy alloys. Hence, with a greater number of components, distortions may decrease since the appearance of numerous atoms of varying sizes and moduli can compensate for the distortion introduced by neighbours. For instance, the paper [63] shows that ternary NiCoCr alloys demonstrate greater distortions and hardening than quaternary ones in a series of multicomponent f.c.c. Fe–Ni–Co–Cr solid solutions.

5. Temperature Dependence of Critical Shear Stress (Yield Stress) in Binary and Multicomponent Solid Solutions with F.C.C. and B.C.C. Lattices. Activation Energy for Movement of Dislocations and Activation Volume

To study further the features peculiar to solid-solution hardening of multicomponent alloys (including HEAs) a detailed analysis of their temperature dependence of the critical shear stress $\tau_{cr}(T)$ (yield stress $\sigma_{0.2}(T)$), quantitative parameters characterizing the athermal and temperature-dependent component — activation energy of dislocation movement and activation volume, compared to pure metals, is necessary.

As known (see, *e.g.*, Refs. [64–67]), critical shear stress τ_{cr} can be described by the following equation:

$$\tau = \tau_a + \tau_T(T, \dot{\varepsilon}), \tag{18}$$

where the first term, τ_a, characterizes athermal component and the second term, $\tau_T(T, \dot{\varepsilon})$, is the temperature-dependent component introduced by barriers that can be overcome by dislocations through thermal fluctuations (T is the temperature and $\dot{\varepsilon}$ is the strain rate).

Following analysis of the papers [64–73], we plotted a schematic temperature dependence (Fig. 7) of critical shear stress $\tau_{cr}(T)$ for metals (curve *1*), of Young's modulus $E(T)$ (curve *2*), and of $\tau_{cr}(T)$ for solid solutions (curve *3*) in Ref. [68].

For metals, the typical temperature dependence of critical shear stress $\tau_{cr}(T)$ (Fig. 7, curve *1* according to Ref. [65]) below T_1 (approximately $0.1T_{melt}$) can be described by straight-line Eq. (19) and that at $T_1 < T < T_2$ (approximately $(0.1–0.2)T_{melt}$) is exponential (20):

$$\tau_T = \frac{U_0 - kT\ln\left(M/\dot{\varepsilon}\right)}{V}, \tag{19}$$

$$\tau_T = \left(3B\dot{\varepsilon}k\frac{T}{V}\right)^{1/3}\exp\left(\frac{U_0}{3kT}\right). \tag{20}$$

where U_0 is the activation energy for the movement of dislocations; V is

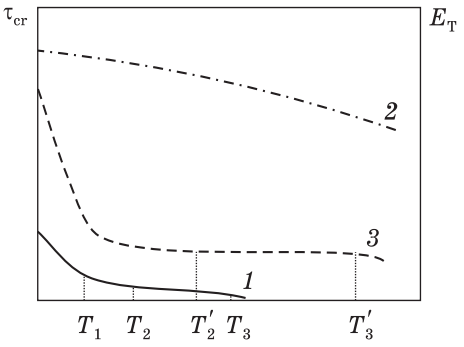

Fig. 7. Schematic temperature-dependent [68] (*1*) critical shear stress (τ_{cr}) for metals, (*2*) Young's modulus (E), and (*3*) critical shear stress (τ_{cr}) for solid solutions. (Plotted considering findings from Refs. [3, 65–72]). Here, T_1 and T_1' are the transition temperatures from linear to exponential dependence, T_2 and T_2' — the transition temperatures to athermal dependence, T_3 and T_3' — the transition temperatures to diffusion-dislocation deformation mechanisms, for metals and solid solutions, respectively

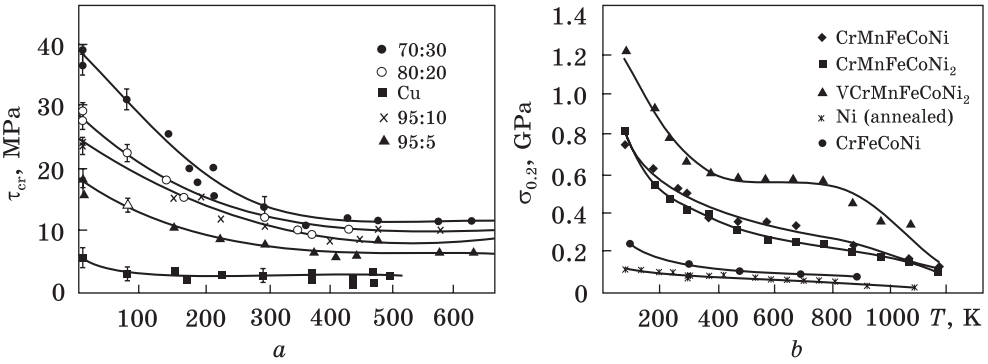

Fig. 8. Temperature dependence of critical shear stress $\tau_{cr}(T)$ for f.c.c. Cu–Zn binary solid solutions [69] (*a*); temperature dependence of yield stress $\sigma_{0.2}(T)$ for multicomponent f.c.c. solid solutions [35] (*b*)

the activation volume for overcoming various potential barriers by dislocations; M, actually, is $\dot{\varepsilon}_0$, $\ln M$ weakly depends on temperature; B is a constant for the singing material and the degree of deformation $\dot{\varepsilon}$, which is indicated by $\tau_{cr}(T)$; k is Boltzmann's constant.

In the temperature range $T < T_2$, hardening is determined by barriers that can be overcome through thermal fluctuations. For pure b.c.c. and f.c.c. metals, the barriers significantly differ in nature [64]. In b.c.c. metals, these are Peierls–Nabarro barriers. The ability of dislocations to overcome these barriers through thermal activation at room temperature and below largely determines the critical shear stress. In f.c.c. metals, the level of Peierls–Nabarro barriers is low. The barriers are forest dislocations and dislocation thresholds. Pure b.c.c. metals have a sharper $\tau_{cr}(T)$ dependence compared to pure f.c.c. metals.

Above T_2 ($\approx 0.2T_{melt}$) for most metals and alloys [64]) and up to T_3 ($(0.33–0.4)T_{melt}$), athermal $\tau_{cr}(T)$ dependence is observed. There is a weak $\tau_{cr}(T)$ dependence resulting from the temperature dependence of elastic modulus E (curve *2*, according to [72]).

Above T_3, diffusion–dislocation strain mechanisms are induced, and the $\tau_{cr}(T)$ dependence is further weakened (for example, [73]).

Temperatures T_2' and T_3' on curve *3*, which demonstrates the schematic dependence of $\tau_{cr}(T)$ for multicomponent solid solutions, are higher than temperatures T_2 and T_3 (curve *1*) and are discussed below.

The paper [35] shows that, compared to pure f.c.c. metals, binary and multicomponent f.c.c. solid solutions demonstrate a sharper dependence of the thermal component in the critical shear stress and a significant increase in its athermal component (Fig. 8). At the same time, the $\tau_{cr}(T)$ dependence for f.c.c. solid solutions with increase in the concentration of doping elements demonstrates 'b.c.c.-like behaviour', where Peierls–

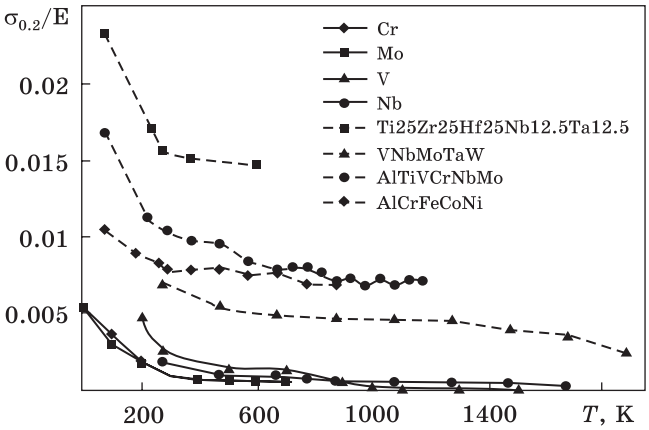

Fig. 9. Temperature dependence of yield stress $\sigma_{0.2}$ normalized to Young's modulus E for multicomponent b.c.c. AlCrFeCoNi, Al TiVCrNbMo, Ti25Zr25 Hf25 Nb12.5Ta12.5, VNbMoTaW alloys and for b.c.c. metals such as chromium, molybdenum, vanadium, and niobium [71]

Nabarro barriers determine it. Similar dependences for the group of f.c.c. HEAs were obtained in [74].

A somewhat more complicated pattern is observed in solid solutions with a b.c.c. lattice. The papers [75–77] show that τ_{cr} decreases (*i.e.*, the thermal component of the dependence $\tau_{cr}(T)$ weakens) in binary solid solutions compared to the base metal (the so-called 'solid-solution softening' occurs) in the region of low concentrations of doping elements at low temperatures. The thermal component in multicomponent b.c.c. solid solutions enhances as compared to pure b.c.c. metals (Fig. 9) [71]. As in the case with f.c.c. solid solutions, the athermal component increases for both binary and multicomponent b.c.c.-solid solutions with greater concentration of the doping element. Note that numerous theories have been put forward, whose systematic analysis is reported in [75], to explain the hardening of binary solutions at low temperatures, *i.e.*, in the temperature range, where the critical shear stress is largely determined by the thermally activated overcoming of Peierls barriers.

According to the methodology developed by Trefilov and Milman [65], the activation energy for the movement of dislocations U_0 and the activation volume V for binary and multicomponent solid solutions with f.c.c. and b.c.c. lattices were calculated, and a comparative analysis with the values for pure metals was carried out in Refs. [35, 71]. This methodology determines the thermal activation parameters using only the $\tau_{cr}(T)$ curve (or the $\sigma_{0.2}(T)$ curve) without the need to vary the strain rate, contrastingly to well-known Seeger–Konrad technique [66, 67].

As shown in Ref. [35], the activation energy for the movement of dislocations U_0 changes relatively weakly, while the activation volume V mainly decreases (Table 1) in transition from pure f.c.c. metals to solid solutions. Thus, for example, U_0 is of 0.11 eV for Cu, 0.18 eV for Cu–30Zn, and 0.21 eV for CrMnFeCoNi, while the activation volume V de-

creases from $2450 \cdot 10^{24}$ cm^3 for Cu to $520 \cdot 10^{24}$ cm^3 for Cu–30Zn and to $114 \cdot 10^{24}$ cm^3 for CrMnFeCoNi.

In the case of the b.c.c. crystal lattice (Table 2), U_0 in both multicomponent and binary solid solutions is comparable to the values for pure metals: *e.g.*, 0.22 eV for Fe, 0.20 eV for Fe–4.03Mo, and 0.22 eV for AlTiVCrNbMo. However, the activation volume V in b.c.c. alloy is significantly lower in multicomponent solid solutions than it is in binary ones, in which the thermal component is weakened in comparison with pure metals. This volume can be compared to (or is even lower than) the values for b.c.c. metals: *e.g.*, $84 \cdot 10^{24}$ cm^3 for Fe, $18.7 \cdot 10^{24}$ cm^3 for AlTiVCrNbMo, and $176 \cdot 10^{24}$ cm^3 for Fe–4.03 Mo.

Table 1. **Activation energy for the movement of dislocations U_0, activation volume V, and average size mismatch $\Delta a/a$ for f.c.c. binary and multicomponent solid solutions and metals [35]**

Material	U_0, eV	$V \cdot 10^{24}$, cm^3	$\Delta a/a$
Cu	0.11	2450	
Cu–5Zn	0.13	860	0.004
Cu–30Zn	0.18	520	0.019
Cu–10Ni	0.2	1990	0.0045
Cu–50Ni	0.26	820	0.0127
Ag	0.07	10560	
Ag–0.5In	0.11	7150	0.0008
Ag–4In	0.22	4490	0.0064
Ni	0.19	800	
Ni–30Cu	0.23	460	0.0108
CrFeCoNi	0.21	194	0.008
CrMnFeCoNi	0.21	114	0.015
$CrMnFeCoNi_2$	0.24	113	0.014
$VCrMnFeCoNi_2$	0.32	111	0.038

Table 2. **Activation energy for the movement of dislocations U_0, activation volume V, and average size mismatch $\Delta a/a$ for b.c.c. binary and multicomponent solid solutions and metals [71]**

Material	U_0, eV	$V \cdot 10^{24}$, cm^3	$\Delta a/a$
Fe	0.22	84	
Cr	0.20	44	
Mo	0.19	45	
Fe–4.03 Mo	0,20	176	0.0075
$Ti_{25}Zr_{25}Hf_{25}Nb_{12.5}Ta_{12.5}$	0.18	45	0.0391
VNbMoTaW	0.16	—	0.0281
AlTiVCrNbMo	0.22	18.7	0.04

Tables 1 and 2 also show that there is an undoubted correlation between the increase in lattice picoscale distortions, described by the average size mismatch $\Delta a/a$, and the decrease in the activation volume V.

The thermal activation analysis indicates that the activation volume V decreases in binary and multicomponent f.c.c. solid solutions and multicomponent b.c.c.-solid solutions compared to pure metals mainly because of a shorter distance between the anchor points of the dislocation line. Accordingly, the resistance to the movement of dislocations from the lattice side ('friction' force) increases, leading to enhancement of the thermal component in the yield stress.

The difference in the absolute values of the activation volume V in b.c.c. and f.c.c. metals (Tables 1 and 2) is associated with the distinct natures of the barriers that are overcome by dislocations in these metals through thermal fluctuations when temperature decreases below $(0.15–0.2)T_{melt}$ (in [K]). Thus, in b.c.c. metals, dislocations overcome the Peierls barriers through the nucleation and displacement of paired bends. In f.c.c. metals, the Peierls barriers are low, and the temperature–rate dependence of yield stress is controlled by barriers of different nature: this is an intersection of forest dislocations in pure f.c.c. metals, while an increase in frictional forces is obviously due to the interaction of dislocations with impurity atoms in doped alloys.

It should be noted that the above approaches to the assessment of solid-solution hardening in binary and multicomponent solid solutions involve analysis of data obtained at room temperature, while we believe that data obtained at the temperatures of incipient athermal hardening would be more correct in this case.

6. 'Plateau' on the Temperature Dependence of Critical Shear Stress (Yield Stress) in Solid Solutions

As seen from Figs. 7 (curve *3*), 8, and 9, an extended temperature-independent hardening region, the so-called 'plateau', is observed on the temperature dependence of critical shear stress $\tau_{cr}(T)$ (yield stress $\sigma_{0.2}(T)$) for binary and multicomponent solid solutions and some metals at temperatures in the range $T_2' < T < T_3'$.

The appearance of a 'plateau' on the $\tau_{cr}(T)$ dependence for binary solid solutions was pointed out in Refs. [69, 70]. It is indicated that while τ_{cr} is determined by the 'athermal' component at temperatures approximately above T_{melt} for pure metals and weakly decreases along the $\tau_{cr}(T)$ dependence (Fig. 7, curve *1*) because of the temperature dependence of the elastic modulus E (curve *2*), τ_{cr} for solid solutions does not depend on temperature in the range $(0.33–0.66)T_{melt}$ $(T_2' < T < T_3')$ and a 'plateau' appears on the $\tau_{cr}(T)$ dependence. However, in some cases, a 'plateau' is observed not only on the $\tau_{cr}(T)$ dependence for solid solutions but also for

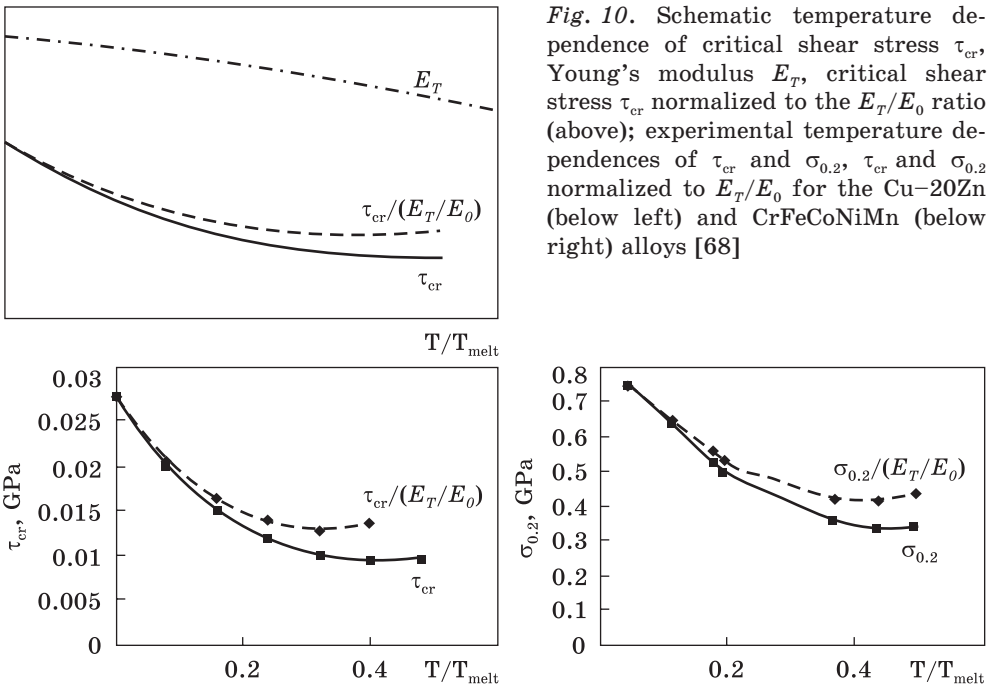

Fig. 10. Schematic temperature dependence of critical shear stress τ_{cr}, Young's modulus E_T, critical shear stress τ_{cr} normalized to the E_T/E_0 ratio (above); experimental temperature dependences of τ_{cr} and $\sigma_{0.2}$, τ_{cr} and $\sigma_{0.2}$ normalized to E_T/E_0 for the Cu–20Zn (below left) and CrFeCoNiMn (below right) alloys [68]

pure metals, for example, pure copper (Fig. 8, *a*). It should be noted that the 'plateau' extends to $\approx 0.6T_{melt}$ for some medium- and high-entropy alloys, such as Nb25Mo25Ta25W25 and V20Nb20Mo20Ta20W20, while it extends only up to $\approx 0.35T_{melt}$ [78] in conventional well-known creep-resistant alloys, such as Inconel and Haynes ones. This is indicative of the fundamental possibility of developing a new generation of high-temperature creep-resistant materials from multicomponent solid solutions.

At the same time, work [67] showed that, since the decrease in Young's modulus with increasing temperature [72, 79–81] should lead to a decrease in the critical shear stress, the presence of a 'plateau' on the dependence of $\tau_{cr}(T)$ is, in fact, anomalous. A 'plateau' may be observed only on the temperature dependence of τ_{cr} normalized to the E_T/E_0 ratio (where E_T and E_0 are the elastic moduli at T and 0 K, respectively) (Fig. 10). Note that the paper [66] also draws attention to the fact that a plateau should be observed on the $\tau_{cr}(T)/G(T)$ dependence but not the $\tau_{cr}(T)$ dependence.

The analysis conducted in Ref. [68] testifies that the factor that compensates for the decrease in τ_{cr} associated with the reduction in the elastic modulus for pure metals is an increase in the root-mean-square displacements of atoms from ideal lattice positions resulting from a linear growth in dynamic distortions with temperature [82]. In multicomponent solid solutions, besides an increase in the root-mean-square displacements of atoms, the $\tau_{cr}(T)$ dependence in the temperature range where a 'plateau' is obser-

ved can also be influenced by effects similar to dynamic strain ageing, which are accompanied by unequal movement of atoms from different elements.

Effects of dynamic strain ageing in HEAs are described, for example, in Refs. [83–86]. Noteworthy data are data reported in the papers showing that the temperature range of effects similar to Portevin–Le Chatelier effect expands as the composition of the alloy becomes more complex.

For example, the paper [84] notes that, while the CoNi alloy shows no serration behaviour in stress strain curves during tests in the range 300–700 °C at a strain rate of $1 \cdot 10^{-4}$ s^{-1}, the CoFeNi alloy shows a serration behaviour at 400 and 500 °C, the CoCrFeNi alloy at 300, 400, 500, and 600 °C, and the CoCrFeMnNi alloy at 300, 325, 350, 375, 400, 500, 600, and 620 °C. The paper [86] reports on the effects of dynamic strain aging in the 18Cr–9Ni–W–Nb–VN austenitic stainless steel at a strain rate ranging from $6.7 \cdot 10^{-6}$ to $1.3 \cdot 10^{-2}$ s^{-1} at temperatures varying from 530 to 680 °C. It is shown that tungsten, niobium, and vanadium additions contribute to the expansion of the temperature range, over which the effects of dynamic strain ageing are manifested from 350 to 740 °C.

When temperature increases, there is a transition from dislocation to dislocation–diffusion strain mechanisms associated with dislocation climb, intergranular sliding. These processes limit the upper temperature, at which a 'plateau' is manifested.

7. Conclusions

(i) Most previous publications regard solid-solution hardening in binary alloys as athermal, which can be described by the following equation: $\Delta\tau(c) = BGc^n(c)$, where τ is the critical shear resistance; B is a coefficient that depends on the parameters of modulus and size mismatch between the atoms that form the solid solution; G is the shear modulus; and c is the concentration of the doping element. For diluted solid solutions, $n = 1/2$ or $2/3$ (when dislocations bend between clusters of dissolved atoms according to Labusch's model). At high concentrations, $n = 1$ and, then, hardening is $\Delta\tau(c) \propto c$.

For alloys with unlimited solubility, $\Delta\tau(c) \propto c(1 - c)$. Considering the inhomogeneous distribution of atoms in a solid solution, hardening is well described by a third-order polynomial [39].

(ii) Models of solid-solution strengthening in multicomponent (high-entropy) solutions based on the Labusch's model (*e.g.*, Refs. [22–24, 44–47]) do not seem to be fully justified, since abnormally high solid-solution hardening in such solutions is similar in nature to hardening in concentrated binary solid solutions and is determined by the averaged resistance to the movement of dislocations, resulting from the presence of lattice picoscale distortions induced by atoms of the alloy components through the size and modulus mismatch.

(iii) The root-mean-square displacements of atoms from ideal lattice positions, $\sqrt{U^2}$, oriented perpendicularly to the slip plane of dislocations, should be used as a measure of the alloy lattice distortion. These displacements are determined by x-ray diffraction and characterized by the intensity of reflections (111) and (222) for f.c.c. lattices and reflections (110) and (220) for b.c.c. lattices. Solid-solution hardening can be defined as $\Delta\tau = k_1 G\sqrt{U^2}/d_{hkl}$ (where k_1 = const and d_{hkl} is interplanar spacing).

Microdistortions $\varepsilon = \Delta d/d$ can be another empirical way of determining the degree of lattice distortion using precision x-ray analysis. In this case, solid-solution hardening is $\Delta\tau = \alpha\varepsilon G$, where α = const.

(iv) The lattice picoscale distortions in binary f.c.c. and multicomponent f.c.c. and b.c.c. solid solutions increase the athermal component in shear stress τ_a and substantially enhance the $\tau_{cr}(T)$ dependence. The effect of a sharp increase in the temperature dependence for f.c.c. solid solutions is called 'b.c.c.-like behaviour'.

(v) Solid-solution hardening in binary and multicomponent alloys is peculiar in that there is an extended athermal 'plateau' on the temperature dependence of critical shear stress $\tau_{cr}(T)$ (yield stress $\sigma_{0.2}(T)$) above $(0.2–0.35)T_{melt}$. Taking into account the temperature dependence of elastic moduli, the presence of a 'plateau' for solid solutions and some pure metals (*e.g.*, Cu) is anomalous. The factors compensating for the effect of the decrease in the elastic moduli with temperature on the $\tau_{cr}(T)$ dependence are as follow:

• in pure metals is the growth of the root-mean-square displacements of atoms from ideal lattice positions with temperature (dynamic distortions of the crystal lattice);

• in binary and multicomponent solid solutions, in addition to the growth of dynamic distortions of the crystal lattice, are the effects of dynamic deformation ageing; note that the 'plateau' length for high-entropy alloys can reach $(0.5–0.6)T_{melt}$.

The findings presented in the paper can be useful in the creation of multicomponent materials (medium- and high-entropy ones) with a high complex of physical and mechanical properties (in particular, strength, plasticity, heat resistance, and wear resistance).

REFERENCES

1. N.F. Mott and F.R.N. Nabarro, *Report of a Conference on the Strength of Solids* (London: The Physical Society: 1948), p. 1.
2. J. Friedel, *Dislocations* (Oxford: Pergamon: 1964), p. 379.
3. P. Haasen, Mechanical Properties of Solid Solutions, *Physical Metallurgy (Fourth, Revised and Enhanced Edition)* (Eds. R.W. Cahn and P. Haasen) (Elsevier: 1996), Vol. **3**, Ch. 23, p. 2009;
https://doi.org/10.1016/B978-044489875-3/50028-4
4. J.P. Hirth and J. Lothe, *Theory of Dislocations* (New York: McGraw-Hill: 1968).

5. R.L. Fleischer and W.R. Hibbard, *Conference on Relation of Structure to Mechanical Properties of Metals* (Teddington: National Physical Laboratories National Physical Laboratories: 1964), p. 262.
6. M. Z. Butt and P. Feltham, *J. Mater. Sci.*, **28**: 2557 (1993); https://doi.org/10.1007/BF00356192
7. J.W. Yeh, S.K. Chen, S.J. Lin, J.Y. Gan, T.S. Chin, T.T. Shun, and C.H. Tsau, *Adv. Eng. Mater.*, **6**, No. 5: 299 (2004); https://doi.org/10.1002/adem.200300567
8. J.W. Yeh, Yu-L. Chen, Su-J. Lin, and S.-K. Chen, *Mater. Sci. Forum*, **560**: 1 (2007); https://doi.org/10.4028/www.scientific.net/MSF.560.1
9. K.H. Huang, *A Study on the Multi-Component Alloy System Containing Equal-mole Elements* (Thesis for Master Degree) (National Tsing Hua University in Taiwan: 1995).
10. Y. Zhang and Y. J. Zhou, *Mater. Sci. Forum*, **561–565**: 1337 (2007); https://doi.org/10.4028/www.scientific.net/MSF.561-565.1337
11. Y. Zhang, *Mater. Sci. Forum*, **654–656**: 1058 (2010); https://doi.org/10.4028/www.scientific.net/MSF.654-656.1058
12. S.A. Firstov, V.F. Gorban', and N.A. Krapivka, *Vestnik SamGTU. Ser. Fiziko-Matematicheskie Nauki* (Samara: 2009), p. 19 (in Russian).
13. S. Praveen and H.S. Kim, *Adv. Eng. Mater.*, **20**, No. 1: 1700645 (2017); https://doi.org/10.1002/adem.201700645
14. H. Zhang, Y. Zhao, S. Huang, S. Zhu, F. Wang, and D. Li, *Materials*, **12**, 720: 2 (2019); https://doi.org/10.3390/ma12050720
15. Y. Chen, Yu. Li, X. Cheng, C. Wu, Bo Cheng, and Z. Xu, *Materials*, **11**, 208: 2 (2018).
16. O.N. Senkov, G.B. Wilks, D.B. Miracle, C.P. Chuang, and P.K. Liaw, *Intermetallics*, **18**: 1758 (2010). https://doi.org/10.1016/j.intermet.2010.05.014
17. M.-H. Tsai, *Entropy*, **18**: 252 (2016); https://doi.org/10.3390/e18070252
18. D.B. Miracle and O.N. Senkov, *Acta Mater.*, **122**: 448 (2017); https://doi.org/10.1016/j.actamat.2016.08.081
19. Yu.-S. Tian, W. Zhou, Q. Tan, M. Wu, S. Qiao, G. Zhu, An. Dong, Da Shu, and B. Sun, *Trans. Nonferrous Met. Soc. China*, **32**: 3487 (2022).
20. A.C. Yeh, T.K. Tsao, Y.J. Chang, K.C. Chang, J.W. Yeh, M.S. Chiou, S.R. Jian, C.M. Kuo, W.R. Wang, and H. Murakami, *Int. J. Metall. Mater. Eng.*, **1**: 107 (2015); https://doi.org/10.15344/2455-2372/2015/107
21. H.M. Daoud, A.M. Manzoni, N. Wanderka, and U. Glatzel, *JOM*, **67**: 2271 (2015); https://doi.org/10.1007/s11837-015-1484-7
22. I. Toda-Caraballo and P.E.J. Rivera-Díaz-del-Castillo, *Acta Mater.*, **85**: 14 (2015); https://doi.org/10.1016/j.actamat.2014.11.014
23. C. Varvenne, A. Luque, and W.A. Curtin, *Acta Mater.*, **118**: 164 (2016); https://doi.org/10.1016/j.actamat.2016.07.040
24. Z.G. Wu, Y.F. Gao, and H.B. Bei, *Acta Mater.*, **120**: 108 (2016); https://doi.org/10.1016/j.actamat.2016.08.047
25. N.L. Okamoto, K. Yuge, K. Tanaka, H. Inui, and E.P. George, *AIP Advances*, **6**, No. 12: 125008 (2016); https://doi.org/10.1063/1.4971371
26. F. Moitzi, L. Romaner, A.V. Ruban, and O.E. Peil, *Phys. Rev. Mater.*, **6**: 103602 (2022); https://doi.org/10.1103/PhysRevMaterials.6.103602

27. S.I. Rao, C. Woodward, B. Akdim, E. Antillon, T.A. Parthasarathy, and O.N. Senkov, *Scripta Mater.*, **172**: 135 (2019); https://doi.org/10.1016/j.scriptamat.2019.07.025
28. H.L. Zhang, D.D. Cai, X. Sun, H. Huang, S. Lu, Y.Z. Wang, Q.M. Hu, L. Vitos, and X.D. Ding, *J. Mater. Sci. Technol.*, **121**: 105 (2022); https://doi.org/10.1016/j.jmst.2021.11.076
29. R.L. Fleischer, Solid-Solution Hardening, *The Strengthening of Met*als (Eds. D. Peckner) (New York: Reinhold Publishing Corp.: 1964), p. 93.
30. R.A. Labusch, *Phys. Stat. Sol.*, **41**: 659 (1970); https://doi.org/10.1002/pssb.19700410221
31. H. Suzuki, *Strength of Metals and Alloys* (Eds. H. J. McQueen) (Toronto: Pergamon: 1986), p. 1727.
32. I. Wesemann, A. Hoffmann, T. Mrotzek, and U. Martin, *17th Plansee Seminar*, **1**: 18/1 (2009).
33. S. Takeuchi, *Scripta Metallurgica*, **2**: 481 (1968); https://doi.org/10.1016/0036-9748(68)90177-4
34. H. Hattendorf and A. R. Büchner, *Zeitschrift für Metallkunde*, **83**: 690 (1992); https://doi.org/10.1515/ijmr-1992-830910
35. S.A. Firstov and T.G. Rogul, *Metallofiz. Noveishie Tekhnol.*, **39**, No. 1: 33 (2017) (in Russian); https://doi.org/10.15407/mfint.39.01.0033
36. S. Patinet and L. Proville, *Phys. Rev. B*, **78**: 104109:1 (2008); https://doi.org/10.1103/PhysRevB.78.104109
37. A. Seeger, Theorie der Kristallplastizität, **IV**, *Verfestigung und Gleitmechanismus dichtest gepackter Metalle und Legierungen. Z. Naturforschg*, **11a**: 985 (1956).
38. G. Sachs and J. Weerts, *Tensile Tests on Gold–Silver Crystals* (Berlin–Dahlem: Communication from the Kaiser-Wilhelm-Institut für Metallforschung: 1930), p. 473.
39. S.A. Firstov and T.G. Rogul, *Dopov. Nac. Akad. Nauk Ukr.*, **8**: 58 (2018) (in Russian); https://doi.org/10.15407/dopovidi2018.08.058
40. B. Chalmers, *Physical Metallurgy* (New York: Wiley: 1959), p. 468.
41. I. Milne and R.E. Smallman, *Trans. AIME*, **242**: 120 (1968).
42. O.N. Carlson and A.L. Eustice, *Vanadium–Chromium Alloy System* (Iowa State University Ames Laboratory Technical Reports: 1959), p. 12; https://lib.dr.iastate.edu/ameslab_isreports/12
43. L.A. Gypen and A. Deruyttere, *J. Mater. Sci.*, **12**, No. 5: 1028 (1977); https://doi.org/10.1007/BF00540988
44. L.A. Gypen and A. Deruyttere, *J. Mater. Sci.*, **12**, No. 5: 1034 (1977); https://doi.org/10.1007/BF00540988
45. O.N. Senkov, J.M. Scott, S.V. Senkova, D.B. Miracle, and C.F. Woodwart, *Intermetallics*, **509**: 6043 (2011); https://doi.org/10.1016/j.jallcom.2011.02.171
46. I. Toda-Caraballo, *Scripta Mater.*, **127**: 113 (2017); https://doi.org/10.1016/j.scriptamat.2016.09.009
47. C.R. LaRosa, M. Shiha, C. Varvenneb, and M. Ghazisaeidia, *Materials Characterization*, **151**: 310 (2019); https://doi.org/10.1016/j.matchar.2019.02.034
48. M. Walbrühl, D. Linder, J. Egren, and A. Borgenstam, *Mater. Sci. Eng. A*, **700**: 301 (2017); https://doi: 10.1016/j.mseaa.2017.06.001

49. S.-P. Wanga and J. Xua, *Intermetallics*, **95**: 59 (2018); https://doi.org/10.1016/j.intermet.2018.01.017
50. C.-M. Lin, C.-C. Juan, C.-H. Chang, C.-W. Tsai, and J.-W. Yeh, *J. Alloys Compd.*, **624**: 100 (2015); https://doi.org/10.1016/S1003-6326(19)65054-5
51. S.A. Firstov, T.G. Rogul', N.A. Krapivka, S.S. Ponomarev, V.N. Tkach, V.V. Kovylyaev, V.F. Gorban', and M.V. Karpets, *Russ. Metallurgy (Metally)*, **4**: 285 (2014); https://doi.org/10.1134/S0036029514040028
52. S.A. Firstov, T.G. Rogul', N.A. Krapivka, S.S. Ponomarev, V.V. Kovylyaev, N.I. Danilenko, N.D. Bega, V.I. Danilenko, and S.I. Chugunova, *Powder Metall. Met. Ceram.*, **55**: 225 (2016); https://doi.org/10.1007/s11106-016-9797-9
53. L. Vegard, *Zeitschrift fьr Physik*, **5**, Nr. 1: 17 (1921); https://doi.org/10.1007/BF01349680
54. D. Tabor, *The Hardness of Metals* (Oxford, UK: Clarendon Press: 1951), p. 102.
55. https://studme.org/1258042620681/statistika/srednee_kvadraticheskoe_otklonenie
56. M.A. Baranov and V.M. Sherbakov, *EFTZh* (Ehlektronnyi Fiziko-Tekhnicheskii Zhurnal), **5**: 1 (2010) (in Russian).
57. A.A. Rusakov, *Rentgenografiya Metallov* [Röntgenography of Metals] (Moskva: Atomizdat: 1977), p. 480 (in Russian).
58. J.D. Dunitz, V. Schomaker, and K.N. Trueblood, *J. Phys. Chem.*, **92**: 856 (1988); https://doi.org/10.1021/j100315a002
59. W. Yeh, S.Y. Chang, Y.D. Hong, S.K. Chen, and S.J. Lin, *Mater. Chem. Phys.*, **103**: 41 (2007); https://doi.org/10.1016/j.matchemphys.2007.01.003
60. O.B. Perevalova, A.V. Panin, and E.O. Tyurin, *Fazovyye Perekhody, Uporyadochennyye Sostoyaniya i Novyye Materialy*, **1**: 28 (2013) (in Russian).
61. O.V. Sobol, V.F. Gorban, M.O. Krapivka, T.G. Rogul, and S.O. Firstov, *Powder Metall. Met. Ceram.*, **59**: 715 (2021); https://doi.org/10.1007/s11106-021-00206-4
62. V.F. Gorban, M.I. Danylenko, M.A. Krapivka, and S.A. Firstov, *Powder Metall. Met. Ceram.*, **58**: 469 (2019); https://doi.org/10.1007/s11106-019-00097-6
63. S.A. Firstov, T.G. Rogul', and O.A. Shut, *Powder Metall. Met. Ceram.*, **57**: 161 (2018); https://doi.org/10.1007/s11106-018-9964-2
64. V.I. Trefilov, Yu.V. Milman, and S.A. Firstov, *Fizicheskie Osnovy Prochnosti Tugoplavkikh Metallov* [Physical Fundamentals of Strength of Refractory Metals] (Kiev: Naukova Dumka: 1975), p. 315 (in Russian).
65. Y.V. Mil'man and V.I. Trefilov, *Powder Metal. Met. Ceram.*, **49**: 374 (2010); https://doi.org/10.1007/s11106-010-9248-y
66. A. Seeger, *An International Conference 'Dislocations and Mechanical Properties of Crystals' (September 6–8, 1956, Lake Placid)*, p. 179.
67. H. Conrad, *Yielding and Flow of the B.C.C. Metals at Low Temperatures*, (Aerospace Report No. TDR-169(3240-11)TN-5,7 March, 1963), p. 73.
68. S.O. Firstov and T.G. Rogul, *Metallofiz. Noveishie Tekhnol.*, **44**, No. 1: 127 (2022) (in Ukrainian); https://doi.org/10.15407/mfint.44.01.0127
69. O. Boser, *Metall. Trans.*, **3**: 843 (1972); https://doi.org/10.1007/BF02647658

70. T.E. Mitchell, *Progr. Applied Materials Res.*, **6**: 117 (1964).
71. S.O. Firstov, T.G. Rogul, M.O. Krapivka, and S.I. Chugunova, *Metallofiz. Noveishie Tekhnol.*, **40**, No. 2: 219 (2018) (in Russian); https://doi.org/10.15407/mfint.40.02.0219
72. S.A. Firstov and G.F. Sarzhan, *Ehlektronnaya Mikroskopiya i Prochnost' Materialov: Sb. Nauchn. Trudov* (Kiev: IPM NAN Ukrainy: 2014), vol. **20**, p. 71 (in Russian).
73. Z. Guo, N. Saunders, J.P. Schillй, and A.P. Miodownik, *MRS Int. Materials Research Conf. (June 20, 2008, Chongqing, China)*, p. 9.
74. Z. Wu, H. Bei, G.M. Pharr, and E.P. George, *Acta Mater.*, **81**: 428 (2014); https://doi.org/10.1016/j.actamat.2014.08.026
75. J.R. Stephens and W. R. Witzke, *Alloy Softening in Binary Iron Solid Solutions* (Washington, D.C.: NASA Scientific and Technical Publication, Lewis Research Center: February, 1976).
76. W.C. Leslie, *Metall. Trans.*, **3**: 5 (1972); https://doi.org/10.1007/BF02680580
77. E. Pink and R.J. Arsenault, *Prog. Mater. Sci.*, **24**: 1 (1979); https://doi.org/10.1016/0079-6425(79)90003-3
78. O.N. Senkov, G.B. Wilks, J.M. Scott, and D.B. Miracle, *Intermetallics*, **19**, 5: 698 (2011); https://doi.org/10.1016/j.intermet.2011.01.004
79. D. Zakarian, A. Khachatrian, and S. Firstov, *Metal Powder Rep.*, **74**, No. 4: 204 (2021); https://doi.org/10.1016/j.mprp.2018.12.079
80. B.M. Drapkin, *Metally,* **3**: 193 (1980) (in Russian).
81. V.S. Zolotorevskiy, *Mekhanicheskie Svoistva Metallov* [Mechanical Properties of Metals] (Moskva: Metallurgiya: 1983) (in Russian).
82. Yu.A. Bagarjackij, Ya.M. Golovchiner, and V. Il'na, *Rentgenografiya v Fizicheskom Metallovedenii* [Rцntgenography in Physical Metallurgy] (Moskva: Metallurgiya: 1961) (in Russian).
83. P. Lukac and Z. Trojanova, *J. Mechanical Behavior of Materials*, **4**, No. 1: 71 (1992); https://doi.org/10.1515/JMBM.1992.4.1.71
84. R. Carroll, C. Lee, C.-W. Tsai, J.-W. Yeh, J. Antonaglia, B.A.W. Brinkman, M. LeBlanc, X. Xie, S. Chen, P.K. Liaw, and K.A. Dahmen, *Sci. Rep.*, **5**: 16997 (2015); https://doi.org/10.1038/srep16997
85. B. Wang, X. Huang, A. Fu, Y. Liu, and B. Liu, *Mater. Sci. Eng. A*, **726**: 37 (2018); https://doi.org/10.1016/j.msea.2018.04.071
86. I. Nikulin, R. Kaibyshev, and V. Skorobogatykh, *J. Phys.: Conf. Ser.*, **240**: 1 (2010); https://doi.org/10.1088/1742-6596/240/1/012071

Received 21.03.2024
Final version 26.07.2024

С.О. Фірстов, Т.Г. Рогуль
Інститут проблем матеріалознавства ім. І.М. Францевича НАН України,
вул. Омеляна Пріцака, 3, 03142 Київ, Україна

ОСОБЛИВОСТІ ТВЕРДОРОЗЧИННОГО ЗМІЦНЕННЯ ТА ТЕМПЕРАТУРНОЇ ЗАЛЕЖНОСТІ КРИТИЧНОГО НАПРУЖЕННЯ ЗСУВУ В БІНАРНИХ І БАГАТОКОМПОНЕНТНИХ СПЛАВАХ

Наведено аналіз твердорозчинного зміцнення бінарних і багатокомпонентних твердих розчинів (у тому числі високоентропійних сплавів); розглянуто уявлення про композиційно-кластерну будову бінарних твердих розчинів з необмеженою розчинністю, на основі якого запропоновано рівняння, що описує концентраційну залежність критичного напруження зсуву; наведено результати порівняльного аналізу температурних залежностей критичного напруження зсуву (межі плинності) для низки бінарних та багатокомпонентних твердих розчинів і чистих металів з ОЦК- та ГЦК-ґраткою; описано можливі механізми появи «плато» на температурній залежності критичного напруження зсуву для бінарних і багатокомпонентних твердих розчинів та чистих металів; досліджено специфіку атермічного зміцнення високоентропійних сплавів і запропоновано відносно простий вираз для його оцінювання; розглянуто можливості використання методів рентгенографічного аналізу для визначення середньоквадратичних зміщень атомів з ідеальних положень у вузлах кристалічної ґратки $\sqrt{U^2}$ та мікроспотворень кристалічної ґратки є у багатокомпонентних твердих розчинах.

Ключові слова: бінарні та багатокомпонентні сплави, твердорозчинне зміцнення, межа плинності, критичне напруження зсуву.